Tuijin Jishu/Journal of Propulsion Technology
ISSN: 1001-4055
Vol. 45 No. 3 (2024)

Modelling COVID-19 Dynamics with a Double Dose Vaccination Strategy in India and Its Potential Influence on the Emergence of Future Diseases

Jitendra Rajbhar [1], A.K. Jaiswal [2] ,Rajan Kumar Dubey [3]
[1,2,3]Department of Mathematics and Statistics, *DeenDayal Upadhyaya Gorakhpur University, Gorakhpur, U.P. (India), 273009*

Abstract:- COVID-19 is a contagious disease responsible for millions of deaths annually and represents a significant global public health challenge. Despite ongoing vaccination efforts, the current COVID-19 situation remains worrisome. This study examines a COVID-19 model incorporating a double-dose vaccination strategy to manage the outbreak in India. We conducted a fundamental qualitative analysis of this mathematical model, investigating conditions for positive invariance and boundedness with appropriate initial conditions. We estimated the basic reproduction number (R_0) for disease transmission and identified two equilibrium points: the disease-free equilibrium and the disease-endemic equilibrium. Using the Routh-Hurwitz criteria, we assessed the stability of these equilibria. The disease can be eradicated if $R_0 < 1$; otherwise, it persists in the population. To complement the qualitative analysis, we performed numerical simulations using MATLAB and estimated model parameters. Sensitivity analysis was conducted to explore the relationship between model parameters and mild and critical cases. The simulations demonstrated that a complete vaccination program significantly reduces mild and critical cases and could potentially eradicate the virus from the community. The insights from our analysis may assist public health professionals in implementing the most effective strategies to control the virus outbreak in India.

Keywords*:* India, COVID-19 model, Stability and Sensitivity analysis; Vaccination.

1. Introduction

People around the world are continuously facing significant public health challenges due to the spread of the SARS-CoV-2 virus. Various variants of SARS-CoV-2 have emerged due to its mutation rate and severity. According to the World Health Organization (WHO), as of November 4, 2021, there were approximately 248,467,363 reported cases and 5,027,183 deaths from COVID-19, with 7,027,377,238 vaccine doses administered [1, 2]. Most countries have now implemented second-dose vaccinations and are considering booster doses in the near future. Consequently, studying new infections and virus transmission after vaccination is crucial. Mathematical models are essential for exploring disease transmission dynamics, enabling policymakers to evaluate future health risks. Since the mid-20th century, the transmission dynamics of infectious disease outbreaks have been analyzed using deterministic and stochastic epidemiology models. These models represent real-world scenarios and predict the severity of infectious diseases through mathematical concepts. This research is motivated by the ongoing vaccination efforts to curb the transmission of the novel coronavirus among humans. We have developed a COVID-19 mathematical model to simulate the transmission and progression of the virus following one or two doses of vaccination [3]. The transmission dynamics of epidemiological infectious diseases are universal. Numerous researchers have analyzed the transmission dynamics of the coronavirus and proposed various models [4]. They have studied and expanded the Susceptible–Exposed–Infected–Removed (SEIR) mathematical model by incorporating significant compartments to accurately represent real-world scenarios.

Muller and Muller (2021) presented a modified SEIR model to understand the transmission dynamics of the coronavirus on a college campus. They suggested that contact tracing could be an effective strategy to prevent the disease. Awareness programs and appropriate Hospitalization or isolation of infected individuals is a primary measure to effectively mitigate the COVID-19 pandemic [5]. Kemp et al. (2021) [6] utilized a modified SEIR model to analyze the interplay between vaccinations and social measures, exploring the infection and hospitalization rates. This model identifies the vaccination rates required to achieve herd immunity in 2021, factoring in social interactions . Treesatayapun (2022) [7] enhanced the SEIR model by considering quarantined populations and distinguishing between effectively and ineffectively vaccinated individuals, estimating the optimal vaccination strategy through performance analysis . De León et al. (2020) [8] introduced the SEIARD model to study COVID-19 transmission dynamics. Rafiq et al. (2022) [9] developed a new numerical scheme for a more realistic and accurate outcome of a complex bi-modal nonlinear model. Acheampong et al. (2022) [10] created a modified SEIR model to delineate SARS-CoV-2 transmission dynamics in Ghana and assess the basic reproduction number. Liu et al. (2021) [11] proposed a Bayesian SEIR model to explain transmission dynamics across nine regions of England. Gonzalez-Parra et al. (2021) [12] examined two COVID-19 variants, proposing a mathematical model applicable to new variants. Kassa et al. (2020) [13] discussed mitigation strategies and conducted sensitivity analysis. Sharov (2020) [14] and Tong et al. (2021) [15] demonstrated the effectiveness of lockdowns using the SIR model and its extensions. Pai et al. (2020) [16] evaluated the impact of India's lockdown on COVID-19 transmission dynamics. Huang et al. (2021) [17] showed that a combined strategy of vaccination and physical distancing is more effective than stay-at-home orders. Sahin and Sahin (2020) [18] compared three models—the grey model (GM), nonlinear grey Bernoulli model (NGBM), and fractional nonlinear grey Bernoulli model (FANGBM)—to accurately predict COVID-19 case numbers.

Shayak et al. (2021) [19] presented a multi-wave solution based on high and low basic reproduction numbers. Some researchers incorporated the effect of vaccines into their models to better represent disease transmission dynamics using SIR and SEIR models with a two-phase vaccination process. These models assumed that individuals who received the first vaccine dose had partial protection and could still become susceptible, while those with the second dose had almost zero infection risk. Kuddus et al. (2021) [20] studied the impact of double-dose vaccination rates on measles transmission, finding that the transmission rate from susceptible to exposed individuals significantly influenced measles prevalence. Mathematically, disease transmission decreases when the effective reproduction number is below 1. Edward et al. (2015) [21] used a mathematical model to study virus transmission dynamics control. Sen et al. (2021) [22] proposed a new SEIR model to investigate double-dose vaccination feedback. Gomes et al. (2022) [23] discussed vaccination's role in achieving herd immunity. Annas et al. (2020) [24] developed a COVID-19 model considering vaccination and isolation factors. Moore et al. (2021) [25] used a deterministic model to evaluate vaccine efficacy, concluding that double-dose vaccination alone was insufficient to contain outbreaks. They estimated vaccines prevent 85% of infections under the most optimistic assumptions. Optimal vaccination deployment in the community is crucial to prevent disease transmission, reducing infection and death risks. Yang et al. (2021) [26] studied the impact of mitigation, suppression, and multiple rolling interventions to control COVID-19 in the UK and Europe, proposing rolling interventions as an optimal strategy to reduce infections, deaths, and balance healthcare demand. Sah et al. (2021) [27] highlighted the impact of accelerated vaccine distribution on reducing the burden of various COVID-19 variants. Martínez-Rodríguez et al. (2021) [28] investigated vaccination pace and efficacy on COVID-19 prevalence, hospitalizations, and deaths, identifying different burden scenarios. Fuady et al. (2021) demonstrated various vaccine delivery strategies, emphasizing the need for proper distribution to mitigate COVID-19's negative impacts. Rahman and Kuddus (2021) [29] developed an age-structured Susceptible-Latent-Mild-Critical-Removed (SLMCR) model of COVID-19 transmission. Aguilar-Canto et al. (2022) [30] augmented a model with multiple vaccination strategies. Ramos et al. (2021) [31] explored the impact of COVID-19 variants and vaccines using a mathematical model. Arruda et al. (2021) [32] introduced a new epidemic model considering reinfection and multiple viral strains. Leonet et al. (2022) [33] demonstrated an epidemiological model accounting for different SARS-CoV-2 variants and the significance of vaccination. This study presents analytical and numerical simulations of a COVID-19 model to depict disease transmission dynamics [34, 35]. The next-generation matrix

(NGM) technique is used to estimate the basic reproduction number (R_0) for the disease dynamics. We determined the existence and uniqueness of system properties and solutions for disease-free (DFE) and disease-endemic equilibria (DEE). Sensitivity analysis identified the most effective parameters influencing COVID-19 spread. The results guide policymakers on effective steps to mitigate the COVID-19 outbreak in India. The numerical results show that virus transmission significantly decreases when susceptible individuals are fully vaccinated and adhere to health guidelines. The remainder of this paper is structured as follows: Section 2 presents the mathematical formulation of the COVID-19 model. Section 3 discusses the model's existence, uniqueness, equilibrium points, stability, and basic reproduction number. Section 4 includes numerical simulations and sensitivity analysis with appropriate parameter values. Section 5 provides a discussion of the results and concluding remarks.

2. Mathematical Model

In this section, we developed a compartmental model to describe COVID-19 transmission dynamics using a system of ordinary differential equations among various mutually exclusive compartments. Numerous mathematical models have been created to understand COVID-19 transmission dynamics, reflecting their widespread importance. Many of these models have been examined to outline the transmission patterns of infectious diseases. In our model, we divided the total population into nine mutually exclusive compartments: susceptible individuals, $X(t)$, who are uninfected but at risk of infection; first dose vaccinated individuals, $Y(t)$, who still have a risk of infection; second dose vaccinated individuals, $Z(t)$, who have completed both doses on time; and exposed individuals, $W(t)$, who are those who have been Exposed individuals, $W(t)$, are those affected by the disease but who have not yet developed respiratory illness; mild individuals, $A(t)$, are asymptomatic; critical individuals, $B(t)$, show clear COVID-19 symptoms; non-hospitalized individuals, $D(t)$, are not in serious health crisis; hospitalized individuals, $E(t)$, are in critical health and respiratory crisis; and recovered individuals, $F(t)$, have recovered from the disease. The recovery compartment includes those who are COVID-19 negative after treatment, home isolation, no longer in contact with others, or deceased. Figure 1 illustrates the schematic diagram of our proposed COVID-19 model.

The total population size, N(t), is assumed to be constant and well-mixed:

$$N(t) = X(t) + Y(t) + Z(t) + W(t) + A(t) + B(t) + D(t) + E(t) + F(t) \quad \text{....(1)}$$

To maintain a constant population size, all deceased individuals are considered as newborns and are replaced in the susceptible compartment. Natural deaths occur in all compartments at a constant per-capita rate μ and critical health-related deaths occur at a constant per-capita rate α. Individuals who receive the first dose of the vaccine move from the susceptible compartment (X) to the vaccinated compartment (Y) at a constant rate δ. Among the first dose vaccinated population, some revert to the susceptible state at a rate ε, while the remaining progress to the second dose vaccinated state (Z) at a rate ς. Fully vaccinated individuals move to the recovery state (F) from the (Z) state at a constant rate θ. In our model, we assume that the net inflow of the uninfected population to the susceptible state is at a rate of αN. The susceptible population decreases as individuals become infected through contact with the coronavirus at a rate $\beta(A+B)$, where β represents the transmission rate of the virus. The infected individuals then move to the exposed state (W). The exposed compartment contains individuals who may develop mild or critical health conditions. Some exposed individuals transfer to the mild compartment (A) at a rate δ_1, while others progress to the critical compartment at a rate δ_2. Mild individuals may move to the critical compartment at a rate χ due to declining health immunity within a few days, or to the non-hospital compartment at a rate γ. The population in the critical compartment (B) transitions to either the

non-hospital or hospital compartments based on health conditions, at rate υ and ξ, respectively. The recovery rates from the mild (A), non-hospital (D), and hospital (E) compartments are π, ρ, and σ, respectively.

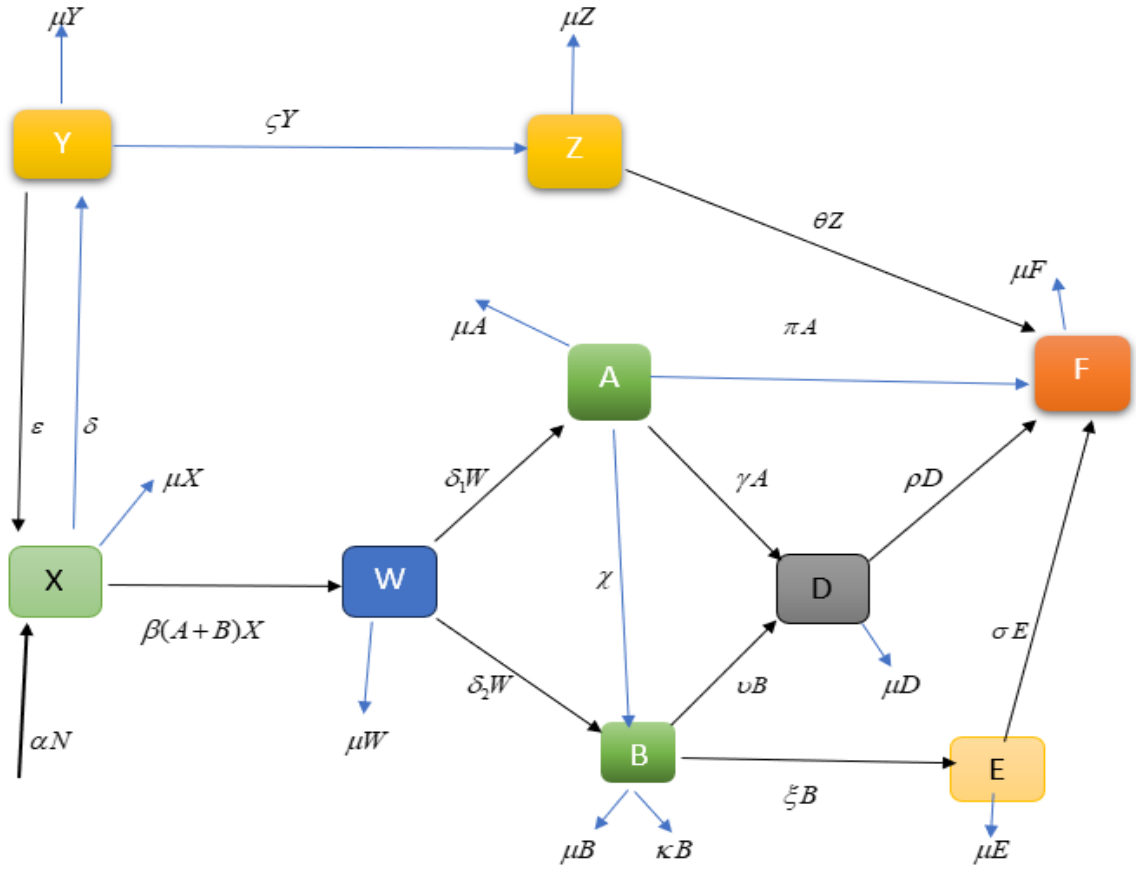

Fig.1. Schematic flow diagram of the disease transmission model.

According to the proposed model, the transmission dynamics of the disease are characterized using the following dynamic variables. The model is outlined by a system of nonlinear ordinary differential equations.

$$\frac{dX}{dt} = \alpha N - \beta X(A+B) - \delta X + \varepsilon Y - \mu X, \qquad \text{.....(2)}$$

$$\frac{dY}{dt} = \delta X - \varepsilon Y - \varsigma Y - \mu Y, \qquad \text{.....(3)}$$

$$\frac{dZ}{dt} = \varsigma Y - \theta Z - \mu Z, \qquad \text{.....(4)}$$

$$\frac{dW}{dt} = \beta X(A+B) - \delta_1 W - \delta_2 W - \mu W, \qquad \text{.....(5)}$$

$$\frac{dA}{dt} = \delta_1 W - \chi A - \pi A - \gamma A - \mu A, \qquad \text{.....(6)}$$

$$\frac{dB}{dt} = \delta_2 W + \chi A - \upsilon B - \xi B - \varpi B - \mu B, \quad \text{.....(7)}$$

$$\frac{dD}{dt} = \upsilon B + \gamma A - \rho D - \mu D, \quad \text{.....(8)}$$

$$\frac{dE}{dt} = \xi B - \sigma E - \mu E, \quad \text{.....(9)}$$

$$\frac{dF}{dt} = \pi A + \rho D + \sigma E + \theta Z - \mu F, \quad \text{.....(10)}$$

With the positive initial conditions:

$X(0) \geq 0, Y(0) \geq 0, Z(0) \geq 0, W(0) \geq 0, A(0) \geq 0, B(0) \geq 0, D(0) \geq 0, E(0) \geq 0$ and $R(0) \geq 0$. ……(11)

3. Quantitative analysis of the model

In this section, we examined the invariant region, the non-negativity of the solution, the existence of equilibria including disease-free and disease-endemic equilibrium points, the basic reproduction number, stability analysis, and sensitivity analysis.

Positive invariance

We analyzed the existence of the solution for the system (2) - (10) with the initial conditions (11) and investigated the non-negativity condition of the dynamic variable for all $t \geq 0$, R_+^9. To establish non-negativity, we present the following theorem.

Theorem 3.1 If the solutions of all dynamic variables $\left(X(t), Y(t), Z(t), W(t).A(t), B(t), D(t), E(t), F(t)\right)$ in the system (2)-(10) with initial conditions (11) satisfy $S(t) > 0, Y(t) > 0, Z(t) > 0, W(t) > 0, A(t) > 0, B(t) > 0, D(t) > 0, E(t) > 0$, and $F(t) > 0$ for all $t > 0$, then the system (2)-(10) is positively invariant and attracting within R_+^9.

Proof. We select Equation (2) from the proposed model, which can be expressed as follows:

$$\frac{dX}{dt} = \alpha N - \beta X(A + B) - \delta X + \varepsilon Y - \mu X$$

$$\frac{dX}{dt} = \alpha N + \varepsilon Y - \tau X \quad \text{.....(12)}$$

Where, $\tau = \beta(A + B) + \varepsilon + \mu$

By integrating the given equation (12), we obtain the following expression.

$$X(t) = X_0 \exp\left(-\int_0^t \tau(u)du\right) + \left(\alpha N + \varepsilon Y\right)\exp\left(-\int_0^t \tau(u)du\right)$$

$$= \int_0^t \left(\exp \int_0^s \tau(v)dv\right) ds \quad \text{.....(13)}$$

Hence the prove.

Positive invariance for all variables

In this section, we establish positive invariance for all other variables. From equation (3) of the model, we derive the following.

$$\frac{dY}{dt} = \delta X - \varepsilon Y - \varsigma Y - \mu Y$$

$$\Rightarrow \quad \frac{dY}{dt} \geq -(\varepsilon + \varsigma + \mu)Y \qquad \text{.....(14)}$$

By solving the above equation (14), we obtain the expression

$$Y(t) \geq Y_0 \exp\left(-\int (\varepsilon + \varsigma + \mu)du\right) > 0 \qquad \text{.....(15)}$$

This shows that $Y(t)$ is non-negative for all t, with Y_0 being the initial value at $t = 0$. Similarly, we can infer that the solution trajectories for the other dynamic variables of the system remain positive for all $t > 0$, and they are:

$$Z(t) \geq Z_0 \exp\left(-\int_0^t (\theta + \mu)du\right) > 0 \qquad \text{.....(16)}$$

$$W(t) \geq W_0 \exp\left(-\int_0^t (\delta_1 + \delta_2 + \mu)du\right) > 0 \qquad \text{.....(17)}$$

$$A(t) \geq A_0 \exp\left(-\int_0^t (\chi + \pi + \gamma + \mu)du\right) > 0 \qquad \text{.....(18)}$$

$$B(t) \geq B_0 \exp\left(-\int_0^t (\upsilon + \xi + \varpi + \mu)du\right) > 0 \qquad \text{.....(19)}$$

$$D(t) \geq D_0 \exp\left(-\int_0^t (\rho + \mu)du\right) > 0 \qquad \text{.....(20)}$$

$$E(t) \geq E_0 \exp\left(-\int_0^t (\sigma + \mu)du\right) > 0 \qquad \text{.....(21)}$$

$$F(t) \geq F_0 \exp\left(-\int_0^t \mu du\right) > 0 \qquad \text{.....(22)}$$

4. Boundedness of the System

We analyzed the model equations (2) through (10) to identify the biologically feasible solution set. The following theorem guarantees that the system's solutions are bounded within the set under non-negative conditions.

Theorem 4.1 The feasible solution set of the system, defined by equations (2) through (10) and subjected to the initial conditions (11) starting in R_+^9, is uniformly bounded in Ω, where $\Omega = \left\{(X, Y, Z, W, A, B, D, E, F) \in R_+^9 : X + Y + Z + W + A + B + D + E + F = N\right\}$ represents the positively invariant region**.**

Proof. By applying the non-negative initial conditions (11) to the system described by equations (2) through (10), we observe that each dynamic variable remains non-negative (as stated in Theorem 3.1). Summing up the equations (2) to (10), we derive the total population size $N(t)$. In the absence of deaths due to COVID-19 or if there are no critical individuals i.e. $C = 0$ [22], we get the following result.

$$\frac{dN}{dt}=\frac{dX}{dt}+\frac{dY}{dt}+\frac{dZ}{dt}+\frac{dW}{dt}+\frac{dA}{dt}+\frac{dB}{dt}+\frac{dD}{dt}+\frac{dE}{dt}+\frac{dF}{dt}$$

$$\Rightarrow \quad \frac{dN}{dt}=\alpha N-\beta X(A+B)-\delta X+\varepsilon Y-\mu X+\delta X-\varepsilon Y-\varsigma Y-\mu Y+\varsigma Y-\theta Z-\mu Z$$
$$+\beta X(A+B)-\delta_1 W-\delta_2 W-\mu W+\delta_1 W-\chi A-\pi A-\gamma A-\mu A+\delta_2 W+\chi A$$
$$-\upsilon B-\xi B-\varpi B-\mu B+\upsilon B+\gamma A-\rho D-\mu D+\xi B-\sigma E-\mu E+\pi A+\rho D$$
$$+\sigma E+\theta Z-\mu F$$

$$\Rightarrow \quad \frac{dN}{dt}=\alpha N-\mu X-\mu Y-\mu Z-\mu W-\mu A-\varpi B-\mu B-\mu D-\mu E-\mu F$$

$$\Rightarrow \quad \frac{dN}{dt}=0$$

By integrating the above equation, we obtain.

$$N(t)=\text{Constant.}$$

Accordingly, given the constant population size, we find that all feasible solutions for each of the dynamic variables X,Y,Z,W,A,B,D,E, and F are bounded within the invariant region.

5. Analysis of equilibria

In this analysis, we identified two equilibrium points in the system: the disease-free equilibrium (DFE) and the disease-endemic equilibrium (DEE). The DFE is reached when the basic reproduction number is less than one (i.e. $R_0<1$), whereas the DEE is reached when the basic reproduction number is greater than one (i.e. $R_0>1$) [22].

5.1 Disease- free equilibrium (DFE) point $\left(\Gamma^0\right)$

In this section, we identify the disease-free equilibrium (DFE) point of the system described by equations (2)-(10), where all disease compartments are set to zero. The model consists of nine compartments: five infected compartments (W,A,B,D,E) and four uninfected compartments (X,Y,Z,F). At the infection-free steady state, W,A,B,D,E and F are all zero. Thus, the DFE point is given by:

$$\Gamma^0=(X^0,Y^0,Z^0,W^0,A^0,B^0,D^0,E^0,F^0)$$

$$=\left(\frac{\alpha N(\varsigma+\varepsilon+\mu)}{(\varsigma+\mu)(\varepsilon+\mu+\delta)-\varepsilon\varsigma},\frac{\delta\alpha N}{(\varsigma+\mu)(\varepsilon+\mu+\delta)-\varepsilon\varsigma},\frac{\delta\mu\varsigma N}{((\mu+\varsigma)(\varepsilon+\mu+\delta)-\varepsilon\varsigma)(\theta+\mu)},0,0,0,0,0,0\right)$$

5.2 Disease-Endemic Equilibrium (DEE) point $\left(\Gamma^*\right)$

In this section, we determine the disease-endemic equilibrium point of the system described by equations (2)-(10), where the disease persists within the population. The endemic equilibrium point is found by setting each equation of the system to zero. It is assumed that all dynamic variables are non-zero at this point, i.e., $X\neq Y\neq Z\neq W\neq A\neq B\neq D\neq E\neq F\neq 0$. Therefore, the endemic equilibrium point is:

$$\Gamma^*=\left(X^*,Y^*,Z^*,W^*,A^*,B^*,D^*,E^*,F^*\right)$$

$$X^* = \frac{(\delta_1+\delta_2+\mu)(\chi+\pi+\gamma+\mu)(\upsilon+\xi+\varpi+\mu)}{\beta\left((\upsilon+\xi+\varpi+\chi+\mu)\delta_1+(\chi+\pi+\gamma+\mu)\delta_2\right)}$$

$$Y^* = \frac{\delta(\delta_1+\delta_2+\mu)(\chi+\pi+\gamma+\mu)(\upsilon+\xi+\varpi+\mu)}{\beta(\varepsilon+\varsigma+\mu)\left((\upsilon+\xi+\varpi+\mu+\chi)\delta_1+(\chi+\pi+\gamma+\mu)\delta_2\right)}$$

$$Z^* = \frac{\delta\varsigma(\delta_1+\delta_2+\mu)(\chi+\pi+\gamma+\mu)(\upsilon+\xi+\varpi+\mu)}{\beta(\theta+\mu)(\varepsilon+\varsigma+\mu)\left((\upsilon+\xi+\varpi+\mu+\chi)\delta_1+(\chi+\pi+\gamma+\mu)\delta_2\right)}$$

$$W^* = \frac{(\delta+\mu)(R_0-1)(\chi+\pi+\gamma+\mu)(\upsilon+\xi+\varpi+\mu)}{\beta\left((\upsilon+\xi+\varpi+\mu+\chi)\delta_1+(\chi+\pi+\gamma+\mu)\delta_2\right)}$$

$$A^* = \frac{(\delta+\mu)(R_0-1)(\upsilon+\xi+\varpi+\mu)\delta_1}{\beta\left((\upsilon+\xi+\varpi+\mu+\chi)\delta_1+(\chi+\pi+\gamma+\mu)\delta_2\right)}$$

$$B^* = \frac{(\delta+\mu)(R_0-1)\left((\chi+\pi+\varpi+\mu)\delta_2+\chi\delta_1\right)}{\beta\left((\upsilon+\xi+\varpi+\mu+\chi)\delta_1+(\chi+\pi+\varpi+\mu)\delta_2\right)}$$

$$D^* = \frac{(\delta+\mu)(R_0-1)\left((\chi+\pi+\gamma+\mu)\delta_2\upsilon+(\upsilon+\xi+\varpi+\mu)\gamma\delta_1+\chi\delta_1\upsilon\right)}{\beta(\rho+\mu)\left((\upsilon+\xi+\varpi+\chi+\mu)\delta_1+(\chi+\pi+\gamma+\mu)\delta_2\right)}$$

$$E^* = \frac{(\delta+\mu)(R_0-1)\left((\chi+\pi+\gamma+\mu)\delta_2+\chi\delta_1\right)\xi}{\beta(\sigma+\mu)\left((\upsilon+\xi+\varpi+\mu+\chi)\delta_1+(\chi+\pi+\gamma+\mu)\delta_2\right)}$$

$$F^* = \frac{(\delta+\mu)(R_0-1)\left(\left((\chi+\pi+\varpi+\mu)\delta_2+\chi\delta_1\right)\left((\sigma+\mu)\rho\upsilon+(\rho+\mu)\sigma\xi\right)+(\upsilon+\xi+\varpi+\mu)\left((\rho+\mu)\pi+\gamma\rho\right)(\sigma+\mu)\delta_1\right)}{+\dfrac{\theta\varsigma\delta(\delta_1+\delta_2+\mu)(\chi+\pi+\gamma+\mu)(\upsilon+\xi+\varpi+\mu)(\sigma+\mu)(\rho+\mu)}{(\varepsilon+\varsigma+\mu)}}$$
$$\mu\beta(\sigma+\mu)(\rho+\mu)(\theta+\mu)\left((\upsilon+\xi+\varpi+\mu+\chi)\delta_1+(\chi+\pi+\gamma+\mu)\delta_2\right)$$

(23)

Restating Eq. (23) indicates that if $R_0>1$, then the disease-endemic equilibrium point $\Gamma^*=\left(X^*,Y^*,Z^*,W^*,A^*,B^*,D^*,E^*,F^*\right)$ lies within the set ζ.

6. Basic Reproduction Number (R_0)

The basic reproduction number can be calculated as the spectral radius of the next generation matrix (NGM) at the disease-free equilibrium point [42]. The NGM can be derived from the product of two matrices, P and Q^{-1}. The matrix P represents the infection transmission rates in the W, A and B compartments, while the matrix Q describes all other transitions between compartments. The matrices P and Q are defined as follows:

$$P=\begin{bmatrix}0 & \beta X^{0} & \beta X^{0}\\ 0 & 0 & 0\\ 0 & 0 & 0\end{bmatrix} \text{ and } Q=\begin{bmatrix}-(\delta_1+\delta_2+\mu) & 0 & 0\\ \delta_1 & -(\chi+\pi+\gamma+\mu) & 0\\ \delta_2 & \chi & (\upsilon+\xi+\varpi+\mu)\end{bmatrix}$$

The next generation matrix is

$$L=P\times(-Q^{-1})$$

$$L=\begin{bmatrix}0 & \beta X^{0} & \beta X^{0}\\ 0 & 0 & 0\\ 0 & 0 & 0\end{bmatrix}\times\frac{\begin{bmatrix}(\chi+\pi+\gamma+\mu)(\upsilon+\xi+\varpi+\varpi) & 0 & 0\\ \delta_1(\upsilon+\xi+\varpi+\mu) & (\upsilon+\xi+\varpi+\mu)(\delta_1+\delta_2+\mu) & 0\\ -(\delta_1\chi+\delta_2(\chi+\pi+\gamma+\mu)) & -\chi(\delta_1+\delta_2+\mu) & -(\delta_1+\delta_2+\mu)(\chi+\pi+\gamma+\mu)\end{bmatrix}}{(\delta_1+\delta_2+\mu)(\chi+\mu+\varpi+\mu)(\upsilon+\xi+\varpi+\mu)}$$

$$L=\frac{\begin{bmatrix}\beta X^{0}\{\delta_1(\upsilon+\xi+\varpi+\mu)-(\delta_1\chi+\delta_2(\chi+\pi+\gamma+\mu))\} & \beta X^{0}\{(\upsilon+\xi+\varpi+\mu)(\delta_1+\delta_2+\mu)-\chi(\delta_1+\delta_2+\mu)\} & -\beta X^{0}(\delta_1+\delta_2+\mu)(\chi+\pi+\gamma+\mu)\\ 0 & 0 & 0\\ 0 & 0 & 0\end{bmatrix}}{(\delta_1+\delta_2+\mu)(\chi+\pi+\varpi+\mu)(\upsilon+\xi+\varpi+\mu)}$$

$$L=\begin{bmatrix}\frac{\beta X^{0}\{\delta_1(\upsilon+\xi+\varpi+\mu)-(\delta_1\chi+\delta_2(\chi+\pi+\gamma+\mu))\}}{(\delta_1+\delta_2+\mu)(\chi+\pi+\varpi+\mu)(\upsilon+\xi+\varpi+\mu)} & \frac{\beta X^{0}\{(\upsilon+\xi+\varpi+\mu)(\delta_1+\delta_2+\mu)-\chi(\delta_1+\delta_2+\mu)\}}{(\delta_1+\delta_2+\mu)(\chi+\pi+\varpi+\mu)(\upsilon+\xi+\varpi+\mu)} & \frac{-\beta X^{0}(\delta_1+\delta_2+\mu)(\chi+\pi+\gamma+\mu)}{(\delta_1+\delta_2+\mu)(\chi+\pi+\varpi+\mu)(\upsilon+\xi+\varpi+\mu)}\\ 0 & 0 & 0\\ 0 & 0 & 0\end{bmatrix}$$

The basic reproduction number (R_0) of the disease is represented by the largest magnitude eigenvalue of the next generation matrix (L). To find this eigenvalue, we solve the characteristic equation $|L-\lambda I|=0$, where λ stands for all possible eigenvalues and I denotes the identity matrix. Thus, the basic reproduction number (R_0) is determined as follows:

$$R_0=\frac{\beta X^{0}\{\delta_1(\upsilon+\xi+\varpi+\mu)-(\delta_1\chi+\delta_2(\chi+\pi+\gamma+\mu))\}}{(\delta_1+\delta_2+\mu)(\chi+\pi+\varpi+\mu)(\upsilon+\xi+\varpi+\mu)}$$

$$R_0=\frac{\beta\alpha N(\varsigma+\varepsilon+\mu)((\upsilon+\xi+\varpi+\mu+\chi)\delta_1+(\chi+\pi+\gamma+\mu)\delta_2)}{((\varsigma+\mu)(\varepsilon+\mu+\delta)-\varepsilon\varsigma)(\delta_1+\delta_2+\mu)(\chi+\pi+\gamma+\mu)(\upsilon+\xi+\varpi+\mu)}$$

7. Stability Analysis of the equilibrium point

In this section, we conducted a stability analysis of both the disease-free equilibrium (DFE) and the disease-endemic equilibrium (DEE).

Theorem: (7.1) The disease-free equilibrium, $\Gamma^{0}=(X^{0},Y^{0},Z^{0},0,0,0,0,0,0)$, of the system (2–10) is locally asymptotically stable when $R_0<1$ and unstable when $R_0>1$.

Proof. To assess the stability of the DFE, $\Gamma^0 = \left(X^0, Y^0, Z^0, 0, 0, 0, 0, 0, 0\right)$, we compute the Jacobian matrix of the system (2) – (11), which is denoted as

$$J = \begin{bmatrix} -\beta(A+B)+\delta+\mu & \varepsilon & 0 & 0 & -\beta X & -\beta X & 0 & 0 & 0 \\ \delta & -(\varsigma+\varepsilon+\mu) & 0 & 0 & 0 & 0 & 0 & 0 & 0 \\ 0 & \varsigma & -(\theta+\mu) & 0 & 0 & 0 & 0 & 0 & 0 \\ -\beta(A+B) & 0 & 0 & -(\delta_1+\delta_2+\mu) & \beta X^0 & \beta X^0 & 0 & 0 & 0 \\ 0 & 0 & 0 & \delta_1 & -(\chi+\pi+\gamma+\mu) & 0 & 0 & 0 & 0 \\ 0 & 0 & 0 & \delta_2 & \chi & -(\upsilon+\xi+\varpi+\mu) & 0 & 0 & 0 \\ 0 & 0 & 0 & 0 & \gamma & \upsilon & -(\rho+\mu) & 0 & 0 \\ 0 & 0 & 0 & 0 & 0 & \xi & 0 & -(\sigma+\mu) & 0 \\ 0 & 0 & \theta & 0 & \pi & 0 & \rho & \sigma & -\mu \end{bmatrix}$$

At the infection-free equilibrium point $\left(\Gamma^0\right)$, the Jacobian matrix has the following form.

$$J\left(\Gamma^0\right) = \begin{bmatrix} -(\delta+\mu) & \varepsilon & 0 & 0 & -\beta X^0 & -\beta X^0 & 0 & 0 & 0 \\ \delta & -(\varsigma+\varepsilon+\mu) & 0 & 0 & 0 & 0 & 0 & 0 & 0 \\ 0 & \varsigma & -(\theta+\mu) & 0 & 0 & 0 & 0 & 0 & 0 \\ 0 & 0 & 0 & -(\delta_1+\delta_2+\mu) & \beta X^0 & \beta X^0 & 0 & 0 & 0 \\ 0 & 0 & 0 & \delta_1 & -(\chi+\pi+\gamma+\mu) & 0 & 0 & 0 & 0 \\ 0 & 0 & 0 & \delta_2 & \chi & -(\upsilon+\xi+\varpi+\mu) & 0 & 0 & 0 \\ 0 & 0 & 0 & 0 & \gamma & \upsilon & -(\rho+\mu) & 0 & 0 \\ 0 & 0 & 0 & 0 & 0 & \xi & 0 & -(\sigma+\mu) & 0 \\ 0 & 0 & \theta & 0 & \pi & 0 & \rho & \sigma & -\mu \end{bmatrix}$$

Now, we need to demonstrate that all the eigenvalues of $J\left(\Gamma^0\right)$ are negative. The 9th column contains only the diagonal element $(-\mu)$, indicating that $(-\mu)$ is one negative eigenvalue. The remaining eigenvalues can be found from the sub-matrix $J_1\left(\Gamma^0\right)$, which is obtained by removing the 9th row and 9th column from $J\left(\Gamma^0\right)$. This results in.

$$J_1\left(\Gamma^0\right) = \begin{bmatrix} -(\delta+\mu) & \varepsilon & 0 & 0 & -\beta X^0 & -\beta X^0 & 0 & 0 \\ \delta & -(\varsigma+\varepsilon+\mu) & 0 & 0 & 0 & 0 & 0 & 0 \\ 0 & \varsigma & -(\theta+\mu) & 0 & 0 & 0 & 0 & 0 \\ 0 & 0 & 0 & -(\delta_1+\delta_2+\mu) & \beta X^0 & \beta X^0 & 0 & 0 \\ 0 & 0 & 0 & \delta_1 & -(\chi+\pi+\gamma+\mu) & 0 & 0 & 0 \\ 0 & 0 & 0 & \delta_2 & \chi & -(\upsilon+\xi+\varpi+\mu) & 0 & 0 \\ 0 & 0 & 0 & 0 & \gamma & \upsilon & -(\rho+\mu) & 0 \\ 0 & 0 & 0 & 0 & 0 & \xi & 0 & -(\sigma+\mu) \end{bmatrix}$$

Similarly, the 3rd, 7th, and 8th columns contain only the diagonal terms $-(\theta+\mu), -(\rho+\mu)$ and $-(\sigma+\mu)$ respectively, which are the negative eigenvalues. The remaining eigenvalues can be determined from the reduced sub-matrix $J_2\left(\Gamma^0\right)$, which is formed by removing the 3rd, 7th, and 8th rows and their corresponding columns from $J_1(\Gamma^0)$.

$$J_2\left(\Gamma^0\right)=\begin{bmatrix} -(\delta+\mu) & \varepsilon & 0 & -\beta X^0 & -\beta X^0 \\ \delta & -(\varsigma+\varepsilon+\mu) & 0 & 0 & 0 \\ 0 & 0 & -(\delta_1+\delta_2+\mu) & \beta X^0 & \beta X^0 \\ 0 & 0 & \delta_1 & -(\chi+\pi+\gamma+\mu) & 0 \\ 0 & 0 & \delta_2 & \chi & -(\upsilon+\xi+\varpi+\mu) \end{bmatrix}$$

This matrix can be expressed in block form as follows:

$$J_2\left(\Gamma^0\right)=\begin{bmatrix} \mathrm{H}_1 & \mathrm{H}_2 \\ \mathrm{H}_3 & \mathrm{H}_4 \end{bmatrix}, \text{Where } \mathrm{H}_1=\begin{bmatrix} -(\delta+\mu) & \varepsilon \\ \delta & -(\varsigma+\varepsilon+\mu) \end{bmatrix}, \mathrm{H}_2=\begin{bmatrix} 0 & -\beta X^0 & -\beta X^0 \\ 0 & 0 & 0 \end{bmatrix}$$

$$\mathrm{H}_3=\begin{bmatrix} 0 & 0 \\ 0 & 0 \\ 0 & 0 \end{bmatrix} \text{ and } \mathrm{H}_4=\begin{bmatrix} -(\delta_1+\delta_2+\mu) & \beta X^0 & \beta X^0 \\ \delta_1 & (\chi+\pi+\gamma+\mu) & 0 \\ \delta_2 & \chi & (\upsilon+\xi+\varpi+\mu) \end{bmatrix}$$

$\because \mathrm{H}_3=\begin{bmatrix} 0 & 0 \\ 0 & 0 \\ 0 & 0 \end{bmatrix}$, then we obtain $\det.\left(\mathrm{H}_1-\lambda I\right)\times\det.\left(\mathrm{H}_4-\lambda I\right)=0$

We can now apply the Routh-Hurwitz stability criterion directly and independently to matrices H_1 and H_4. To do this, we need to show that the trace of each matrix is negative, and for the (2 × 2) matrix H_1, its determinant is positive, while for the (3 × 3) matrix H_4, its determinant is negative. Therefore, for the (2 × 2) matrix H_1, we have:

$$trace\left(\mathrm{H}_1\right)=-(\delta+\mu)-(\varsigma+\varepsilon+\mu)<0$$

and $$\det\left(\mathrm{H}_1\right)=(\delta+\mu)(\varsigma+\varepsilon+\mu)-\delta\varepsilon=\delta\varepsilon+\delta(\varsigma+\mu)+\mu(\varsigma+\varepsilon+\mu)-\delta\varepsilon$$

$$\Rightarrow \quad \det.\left(\mathrm{H}_1\right)=\delta(\varepsilon+\mu)+\mu(\varsigma+\varepsilon+\mu)>0$$

For (3×3) matrix H_4, we get.

Condition (1):

$$trace\left(\mathrm{H}_4\right)=-(\delta_1+\delta_2+\mu)-(\chi+\pi+\gamma+\mu)-(\upsilon+\xi+\varpi+\mu)<0$$

Condition (2):

Sum of minors of matrix H_4 along diagonal

$$=(\delta_1+\delta_2+\mu)(\chi+\pi+\gamma+\mu)+(\delta_1+\delta_2+\mu)(\upsilon+\xi+\varpi+\mu)+(\chi+\pi+\gamma+\mu)(\upsilon+\xi+\varpi+\mu)-\beta X^0(\delta_1+\delta_2)$$

$$=(\delta_1+\delta_2+\mu)(\upsilon+\xi+\varpi+\mu)\left(1-\frac{R_0(\chi+\pi+\gamma+\mu)(\delta_1+\delta_2)}{((\upsilon+\xi+\varpi+\mu+\chi)\delta_1+(\chi+\pi+\gamma+\mu)\delta_2)}\right)+(\delta_1+\delta_2+\mu)(\chi+\pi+\gamma+\mu)+(\chi+\pi+\gamma+\mu)(\upsilon+\xi+\varpi+\mu)>0$$

For $R_0<1$

Condition (3):

$$\det.\left(\mathrm{H}_4\right)=\beta X^0\left((\upsilon+\xi+\varpi+\mu+\chi)\delta_1+(\chi+\pi+\gamma+\mu)\delta_2\right)-(\delta_1+\delta_2+\mu)(\chi+\pi+\gamma+\mu)(\upsilon+\xi+\varpi+\mu)$$

$$= \frac{\beta X^0\left(\left(\upsilon+\xi+\varpi+\mu+\chi\right)\delta_1+\left(\chi+\pi+\gamma+\mu\right)\delta_2\right)}{\left(\delta_1+\delta_2+\mu\right)\left(\chi+\pi+\gamma+\mu\right)\left(\upsilon+\xi+\varpi+\mu\right)}-1$$

$$= R_0 - 1 \text{ for any values of } R_0 < 1.$$

Therefore, the disease-free equilibrium Γ^0 is locally asymptotically stable. if $R_0 < 1$. Conversely, if $R_0 > 1$, Γ^0 will be unstable, meaning that the characteristic equation will have at least one root with a positive real part.

Theorem (7.2) The disease-endemic equilibrium point, Γ^*, of the system (2)-(10) is locally asymptotically stable when $R_0 > 1$.

Proof. We derive the Jacobian matrix of the system (2) – (10) at the equilibrium point $\Gamma^* = \left(X^*, Y^*, Z^*, W^*, A^*, B^*, D^*, E^*, F^*\right)$ which can be written as:

$$J\left(\Gamma^*\right) = \begin{bmatrix}
-\beta\left(A^*+B^*\right)-\delta-\mu & \varepsilon & 0 & 0 & -\beta X^* & -\beta X^* & 0 & 0 & 0 \\
\delta & -\left(\varsigma+\varepsilon+\mu\right) & 0 & 0 & 0 & 0 & 0 & 0 & 0 \\
0 & \varsigma & -\left(\theta+\mu\right) & 0 & 0 & 0 & 0 & 0 & 0 \\
-\beta\left(A^*+B^*\right) & 0 & 0 & -\left(\delta_1+\delta_2+\mu\right) & \beta X^* & \beta X^* & 0 & 0 & 0 \\
0 & 0 & 0 & \delta_1 & -\left(\chi+\pi+\gamma+\mu\right) & 0 & 0 & 0 & 0 \\
0 & 0 & 0 & \delta_2 & \chi & -\left(\upsilon+\xi+\varpi+\mu\right) & 0 & 0 & 0 \\
0 & 0 & 0 & 0 & \gamma & \upsilon & -\left(\rho+\mu\right) & 0 & 0 \\
0 & 0 & 0 & 0 & 0 & \xi & 0 & -\left(\sigma+\mu\right) & 0 \\
0 & 0 & \theta & 0 & \pi & 0 & 0 & \sigma & -\mu
\end{bmatrix}$$

The 9th column of $J\left(\Gamma^*\right)$ includes the diagonal element $-\mu$, indicating that $-\mu$ is a negative eigenvalue. The remaining eigenvalues can be found from the sub-matrix $J_1\left(\Gamma^*\right)$, which is obtained by removing the 9th row and 9th column from $J\left(\Gamma^*\right)$. This results in:

$$J_1\left(\Gamma^*\right) = \begin{bmatrix}
-\beta\left(A^*+B^*\right)-\delta-\mu & \varepsilon & 0 & 0 & -\beta X^* & -\beta X^* & 0 & 0 \\
\delta & -\left(\varsigma+\varepsilon+\mu\right) & 0 & 0 & 0 & 0 & 0 & 0 \\
0 & \varsigma & -\left(\theta+\mu\right) & 0 & 0 & 0 & 0 & 0 \\
\beta\left(A^*+B^*\right) & 0 & 0 & -\left(\delta_1+\delta_2+\mu\right) & \beta X^* & \beta X^* & 0 & 0 \\
0 & 0 & 0 & \delta_1 & -\left(\chi+\pi+\gamma+\mu\right) & 0 & 0 & 0 \\
0 & 0 & 0 & \delta_2 & \chi & -\left(\upsilon+\xi+\varpi+\mu\right) & 0 & 0 \\
0 & 0 & 0 & 0 & \gamma & \upsilon & -\left(\rho+\mu\right) & 0 \\
0 & 0 & 0 & 0 & 0 & \xi & 0 & \left(\sigma+\mu\right)
\end{bmatrix}$$

Similarly, the 3rd, 7th, and 8th columns exclusively contain the diagonal terms $-\left(\theta+\mu\right), -\left(\rho+\mu\right)$ and $-\left(\sigma+\mu\right)$, respectively, which represent the negative eigenvalues. The remaining eigenvalues can be determined from the reduced sub-matrix, $J_2\left(\Gamma^*\right)$ which is obtained by removing the 3rd, 7th, and 8th rows and their corresponding columns from $J_1\left(\Gamma^*\right)$

$$J_2\left(\Gamma^*\right)=\begin{bmatrix} -\beta\left(A^*+B^*\right)-\left(\delta+\mu\right) & \varepsilon & 0 & -\beta X^* & -\beta X^* \\ \delta & -\left(\varsigma+\varepsilon+\mu\right) & 0 & 0 & 0 \\ \beta\left(A^*+B^*\right) & 0 & -\left(\delta_1+\delta_2+\mu\right) & \beta x^* & \beta X^* \\ 0 & 0 & \delta_1 & -\left(\chi+\pi+\gamma+\mu\right) & 0 \\ 0 & 0 & \delta_2 & \chi & -\left(\upsilon+\xi+\varpi+\mu\right) \end{bmatrix}$$

$$\Rightarrow\ J_2\left(\Gamma^*\right)=\begin{bmatrix} -\beta\left(A^*+B^*\right)-Q & \varepsilon & 0 & -\beta X^* & -\beta X^* \\ \delta & -C & 0 & 0 & 0 \\ \beta\left(A^*+B^*\right) & 0 & -G & \beta X^* & \beta X^* \\ 0 & 0 & \delta_1 & -M & 0 \\ 0 & 0 & \delta_2 & \chi & -T \end{bmatrix}$$

Where, $C=\left(\varsigma+\varepsilon+\mu\right)$, $G=\left(\delta_1+\delta_2+\mu\right)$, $M=\left(\chi+\pi+\gamma+\mu\right)$, $T=\left(\upsilon+\xi+\varpi+\mu\right)$ and $Q=\left(\delta+\mu\right)$.

The characteristic equation of $J_2\left(\Gamma^*\right)$ is described as follows:

$$|J_2\left(\Gamma^*\right)-\lambda I|=0$$

$$\Rightarrow\begin{vmatrix} -\beta\left(A^*+B^*\right)-Q-\lambda & \varepsilon & 0 & -\beta X^* & -\beta X^* \\ \delta & -C-\lambda & 0 & 0 & 0 \\ \beta\left(A^*+B^*\right) & 0 & -G-\lambda & \beta X^* & \beta X^* \\ 0 & 0 & \delta_1 & -M-\lambda & 0 \\ 0 & 0 & \delta_2 & \chi & -T-\lambda \end{vmatrix}=0$$

$$\Rightarrow \lambda^5+B_1\lambda^4+B_2\lambda^3+B_3\lambda^2+B_4\lambda+B_5=0 \qquad \text{.....(25)}$$

Where, $O=\left(\varsigma+\mu\right)$, $B_1=\beta\left(A^*+B^*\right)+C+G+M+T+Q$

$$B_2=\left(\left(A^*+B^*\right)\left(C+G+M+T\right)+X^*\left(\delta_1+\delta_2\right)\right)\beta+\left(M+T\right)\left(C+G\right)+\left(G+T+O\right)Q+\left(T+Q\right)M+CG+\varepsilon\mu$$

$$B_3=2X^*\left(A^*+B^*\right)\left(\delta_1+\delta_2\right)\beta^2+\left((A^*+B^*)(C+G+T)+\delta_2X^*\right)M\beta+\left(\delta_1(Q+\chi)+\delta_2Q\right)\beta+(((A^*+B^*)(C+G)+\delta_1X^*)T$$

$$+((A^*+B^*)G+(\delta_1+\delta_2)X^*)C)\beta+GMT+(C+Q)(GM+MT+GT)+(G+M+T)(OQ+\varepsilon\mu).$$

$$B_4=2((\delta_1+\delta_2)C+\delta_2M+\delta_1(T+\chi))(A^*+B^*)X^*\beta^2+(C+Q)(\delta_2M+\delta_1(T+\chi))X^*\beta+(A^*+B^*)(CGM$$

$$+CMT+CGT+GMT)\beta+GMT(C+Q)+(\beta X^*\delta_1+\beta X^*\delta_2+GM+MT+GT)(OQ+\varepsilon\mu).$$

$$B_5 = 2C(\delta_2 M + \delta_1(T+\chi))(A^* + B^*)X^*\beta^2 + ((\delta_2 M + \delta_1(T+\chi)\beta X^* + GMT)(OQ + \varepsilon\mu) + CGMT\beta(A^* + B^*).$$

From equation (25), it is clear that B_1, B_2, B_3, B_4 and B_5 are all greater than zero if A^* and B^* are positive. According to equation (24), A^* and B^* are positive when $R_0 > 1$. Therefore, based on the Routh-Hurwitz stability criterion, the disease-endemic equilibrium point Γ^* is locally asymptotically stable for $R_0 > 1$.

8. Numerical simulation

In this section, we conducted numerical simulations of our proposed model using the Ordinary Differential Equation (ODE) solvers in MATLAB to validate the analytical results. For demonstration purposes, we chose baseline parameter values (refer to Table 1) that align with COVID-19 infection and transmission. Consistent with the analytical results, we identified two equilibrium points: the disease-free equilibrium (Γ^0) and the disease-endemic equilibrium Γ^*

Table 1 Description and estimated value of the model (2–10) parameters.

Parameters	Description	Estimated Value
N	Total Population	163046161
μ	Natural death rate	$\frac{1}{70}$ per year
ε	Progression rate from Y to X	0.095
δ	First dose vaccination rate	0.64
β	Transmission rate	1.0×10^{-6}
ς	Second dose vaccination rate	0.001
θ	Recovery rate due to the second dose of vaccine	0.8
δ_1	Progression rate from W to A	0.007
δ_2	Progression rate from W to B	3.05×10^{-5}
χ	Progression rate from A to B	0.3
ϖ	Disease death rate only for critical compartment	0.125
γ	Progression rate from A to D	0.99
π	Progression rate from A to F	0.02
υ	Progression rate from B to D	0.13
ξ	Progression rate from B to E	0.87
ρ	Recovery rate from D to F	$\frac{1}{42}$
σ	Recovery rate from E to F	$\frac{1}{21}$

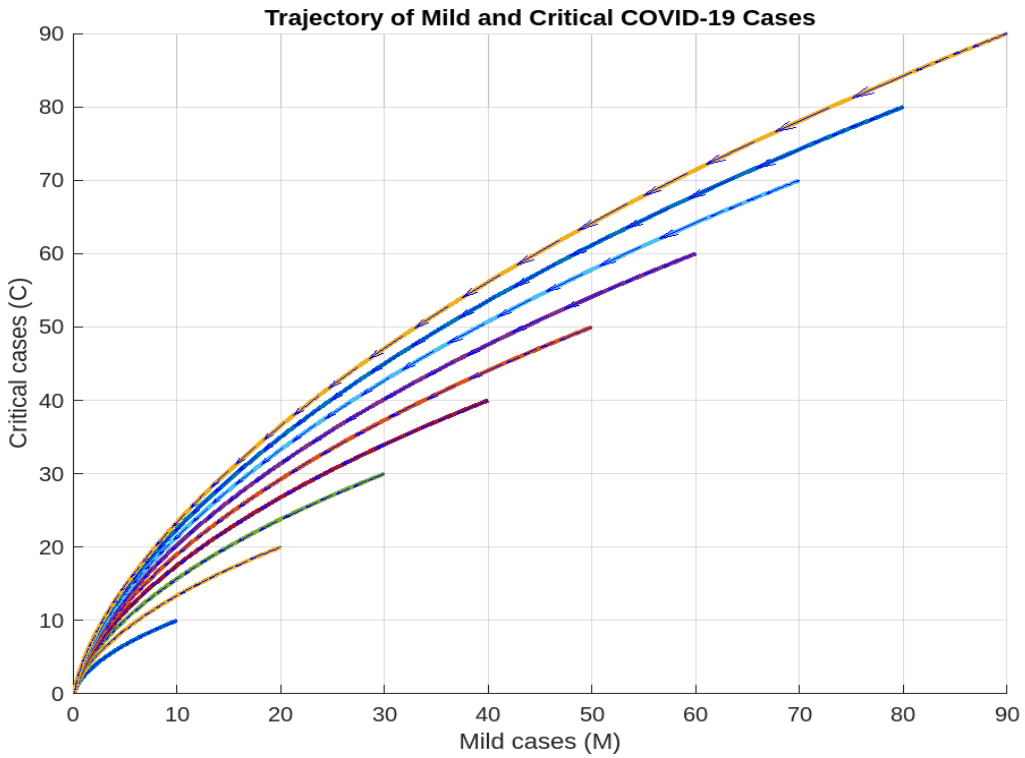

Fig.2. Trajectory of Mild and Critical COVID-19 Cases.

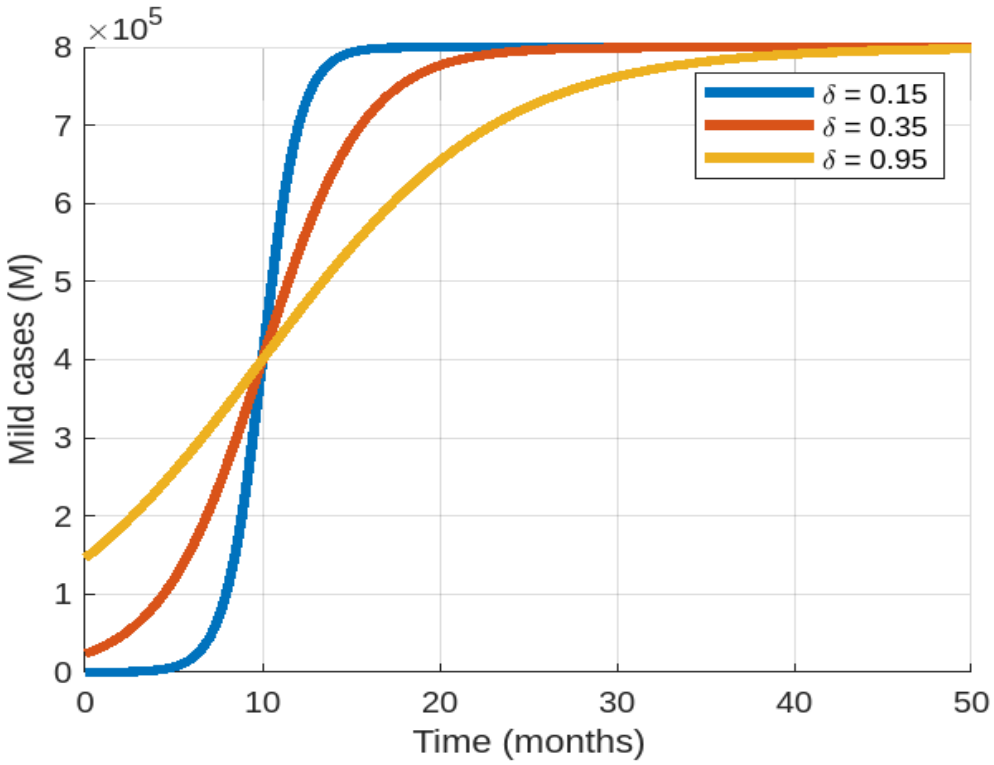

Fig.3. The impact of the first dose of vaccine (δ) on mild cases (A).

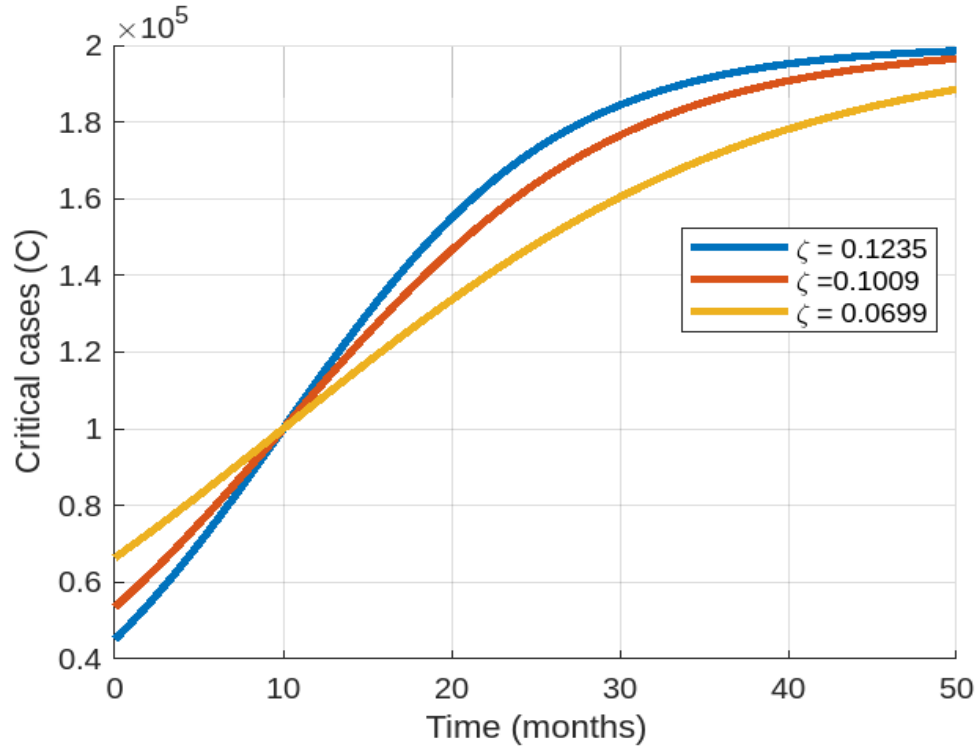

Fig.4. The impact of the second dose of vaccine (ζ) on the critical cases (B).

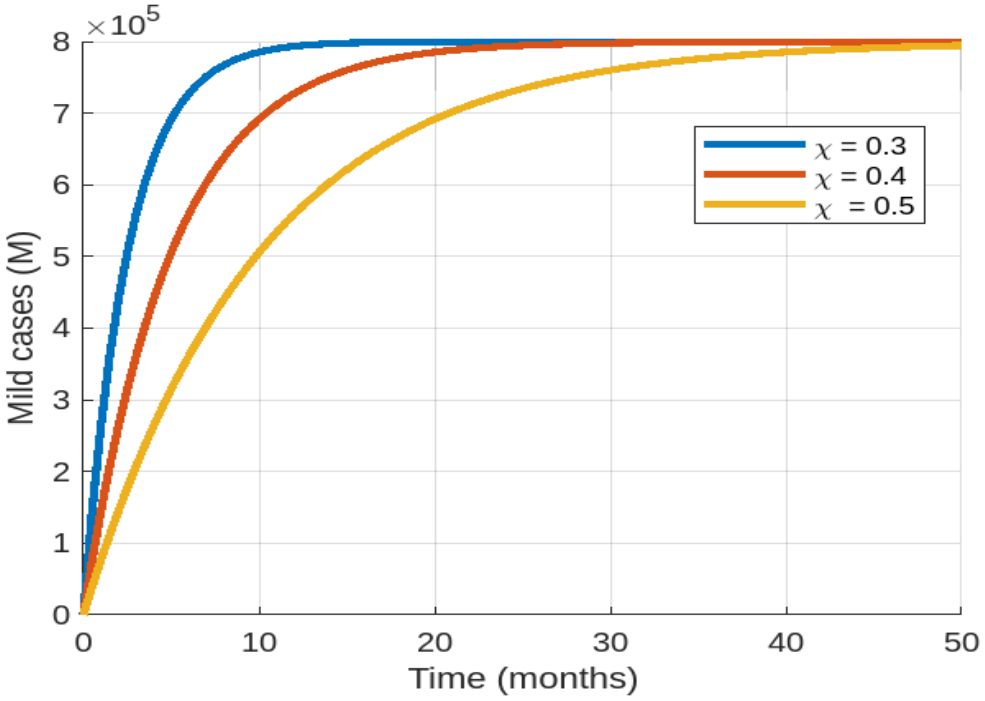

Fig.5. The impact of co-infection on (χ), on the Mild cases (A).

In this section, we conducted numerical simulations of our proposed model using MATLAB's Ordinary Differential Equation (ODE) solvers to support our analytical results. For illustration, we chose baseline parameter values (refer to Table 1) that align with COVID-19 infection and transmission characteristics. Consistent with our analytical findings, we identified two equilibrium points: the disease-free equilibrium (Γ^0) and the disease-

endemic equilibrium Γ^*. From a numerical perspective, the local stability of both equilibrium points was investigated using standard dynamical systems analysis methods. The numerical results of the transmission dynamics for these equilibrium points are shown in Figs. 2. In Fig. 2, we used various initial conditions for all state variables to depict the system trajectories at the disease-free and disease-endemic equilibrium. We found that if the basic reproduction number ($R_0 < 1$) remains below one, the disease-free equilibrium is locally asymptotically stable, indicating that the disease will fade out from the community. Conversely, illustrates the stability of the disease-endemic equilibrium ($R_0 > 1$), showing system trajectories in the A VS B plane originating from different initial conditions, where the virus persists in the community. Figs. 3 illustrate the impact of the first dose vaccine (δ) on mild cases (A) and critical cases (B). These figures indicate that increasing the first dose vaccination rate significantly reduces both mild and critical infection cases. The first dose vaccination rate (δ) negatively correlates with the spread of the disease. From a public health perspective, the first dose vaccine prepares the immune system to combat COVID-19 infection in non-infected individuals, reducing the likelihood of infection despite the presence of the infection rate (ε). Figs. 4 depict the effect of the second dose vaccine (ς) on mild cases (A) and critical cases (B), respectively. These figures demonstrate that both vaccine doses are crucial in reducing outbreak risk. When the second dose vaccination rate (ς) increases from 0.1234 to 0.1009, both mild and critical cases decrease significantly. Moreover, at $\varsigma = 0.0699$, the number of mild and critical cases declines rapidly, as shown in Figs. 4. We recommend that the second dose vaccine is essential for maximum protection against COVID-19, as it continuously stimulates the immune system to produce a large number of antibodies. COVID-19 patients may also have co-infections and can transition from mild (A) to critical (B) cases. Mild individuals experiencing a sudden serious illness are admitted to the hospital and considered critical cases. The co-infection rate (χ) negatively correlates with mild cases (A) and positively correlates with critical cases (B). Fig. 5 shows that mild cases decrease due to co-infection with other diseases, leading to a transition to the critical compartment. As the co-infection rate (χ) positively impacts critical cases, an increase in co-infection leads to an increase in critical cases, as shown in Fig. 5

9. Discussion and conclusion

In the face of rising global COVID-19 cases and ongoing human-to-human transmission, effective vaccination and strategic resource allocation are crucial for public health. Our study introduces a modified SEIR model to analyze COVID-19 transmission dynamics, using both analytical and numerical simulations to identify two equilibrium points: disease-free and disease-endemic. We calculated the basic reproduction number (R_0) and found that both equilibrium points are locally asymptotically stable. When R_0 is less than one, the disease is likely to diminish, while an R_0 greater than one suggests persistence.

The model includes a double-dose vaccination program, reflecting Bangladesh's efforts that began on February 7, 2021. The initial vaccination rate (δ) is vital in preventing outbreaks, as the first dose mitigates severe conditions. Experts recommend completing both doses to enhance antibody production and stimulate memory cells for long-term immunity.

Our analysis shows a positive correlation between R_0 and the transmission rate (β), reinfection rate (ε), and progression rates from exposed to mild (δ_1) and critical (δ_2) cases. Sensitivity analysis highlighted β as the primary factor in disease spread. Thus, reducing the transmission rate is essential, with vaccination being the most effective strategy, potentially reducing transmission by up to 86.1%.

Adherence to health precautions like wearing masks, maintaining safe distances, and frequent hand washing remains crucial. Our numerical simulations indicate that both vaccination doses significantly reduce mild and

critical cases. Consequently, an optimal vaccination program, combined with home isolation for infected individuals, can protect the majority of Bangladesh's population from the virus.

In summary, our study underscores the critical role of vaccination in managing COVID-19 and controlling transmission. Both first and second-dose vaccinations are essential in reducing cases, highlighting the need for a comprehensive vaccination strategy and adherence to health guidelines. Our modified SEIR model demonstrates the stability of disease-free and endemic points, with sensitivity analysis identifying the transmission rate as crucial in disease spread. Vaccination can reduce transmission by up to 86.1%. These insights are vital for managing the current pandemic and preparing for future outbreaks, emphasizing ongoing vaccination efforts in India and providing a framework for future public health strategies.

References:-

[1] Dubey, R. K., & Pandey, R. (2024). Analyzing vaccine efficacy: Stability analysis of SEIR model for Nipah virus in India and Nepal. *Tuijin Jishu/Journal of Propulsion Technology, 45*(4870-4480).

[2] Korber, B., Fischer, W. M., Gnanakaran, S., Yoon, H., Theiler, J., Abfalterer, W., et al. (n.d.). Tracking changes in SARS-CoV-2 spike: Evidence that D614G increases infectivity of the COVID-19 virus.

[3] Dubey, R. K., & Pandey, R. (2023). A SIQRV mathematical model on COVID-19 investigating the combined effect of vaccination and lockdown to control the spread of COVID-19. *International Journal of Food and Nutritional Sciences, 12*, 2835-2850.

[4] Rajbhar, J., Jaiswal, A. K., & Dubey, R. K. (2024). An SIQVR mathematical model on COVID-19 with virus population in the environment: A case study of India. *Journal of Propulsion Technology, 45*(2), 6535-6547.

[5] Musa, S. S., Qureshi, S., Zhao, S., Yusuf, A., Mustapha, U. T., & He, D. (2021). Mathematical modeling of COVID-19 epidemic with effect of awareness programs. *Infectious Disease Modelling, 6*, 448-460.

[6] Kemp, F., Proverbio, D., Aalto, A., Mombaerts, L., Fouquier d'Hérouël, A., Husch, A., et al. (2021). Modelling COVID-19 dynamics and potential for herd immunity by vaccination in Austria, Luxembourg and Sweden. *Journal of Theoretical Biology, 530*, 110874. https://doi.org/10.1016/j.jtbi.2021.110874

[7] Treesatayapun, C. (2022). Epidemic model dynamics and fuzzy neural-network optimal control with impulsive traveling and migrating: Case study of COVID-19 vaccination. *Biomedical Signal Processing and Control, 71*, 103227. https://doi.org/10.1016/j.bspc.2021.103227

[8] Avila-Ponce de Leon, U., Pérez, A. G. C., & Avila-Vales, E. (2020). An SEIARD epidemic model for COVID-19 in Mexico: Mathematical analysis and state-level forecast. *Chaos, Solitons & Fractals, 140*, 110165. https://doi.org/10.1016/j.chaos.2020.110165

[9] Rafiq, M., Ali, J., Riaz, M. B., & Awrejcewicz, J. (2022). Numerical analysis of a bi-modal COVID-19 SITR model. *Alexandria Engineering Journal, 61*(1), 227-235.

[10] Acheampong, E., Okyere, E., Iddi, S., Bonney, J. H. K., Asamoah, J. K. K., & Wattis, J. A. D., et al. (2022). Mathematical modelling of earlier stages of COVID-19 transmission dynamics in Ghana. *Results in Physics, 34*, 105193. https://doi.org/10.1016/j.rinp.2022.105193

[11] Liu, Y., Tang, J. W., & Lam, T. T. Y. (2021). Transmission dynamics of the COVID-19 epidemic in England. *International Journal of Infectious Diseases, 104*, 132-138.

[12] Gonzalez-Parra, G., Martínez-Rodríguez, D., & Villanueva-Mico, R. J. (2021). Impact of a new SARS-CoV-2 variant on the population: A mathematical modeling approach. *Mathematical and Computational Applications, 26*(2), 25.

[13] Kassa, S. M., Njagarah, J. B. H., & Terefe, Y. A. (2020). Analysis of the mitigation strategies for COVID-19: From mathematical modelling perspective. *Chaos, Solitons & Fractals, 138*, 109968. https://doi.org/10.1016/j.chaos.2020.109968

[14] Sharov, K. S. (2020). Creating and applying SIR modified compartmental model for calculation of COVID-19 lockdown efficiency. *Chaos, Solitons & Fractals, 141*, 110295. https://doi.org/10.1016/j.chaos.2020.110295

[15] Tong, Z.-W., Lv, Y.-P., Din, R. U., & Mahariq, I. (2021). Global transmission dynamic of SIR model in the time of SARS-CoV-2. *Results in Physics, 25*, 104253. https://doi.org/10.1016/j.rinp.2021.104253

[16] Pai, C., Bhaskar, A., & Rawoot, V. (2020). Investigating the dynamics of COVID-19 pandemic in India under lockdown. *Chaos, Solitons & Fractals, 138*, 109988. https://doi.org/10.1016/j.chaos.2020.109988
[17] Huang, B., Wang, J., Cai, J., Yao, S., Chan, P. K. S., Tam, T.-W., et al. (2021). Integrated vaccination and physical distancing interventions to prevent future COVID-19 waves in Chinese cities. *Nature Human Behaviour, 5*(6), 695-705.
[18] Sahin, U., & Sahin, T. (2020). Forecasting the cumulative number of confirmed cases of COVID-19 in Italy, UK and USA using fractional nonlinear grey Bernoulli model. *Chaos, Solitons & Fractals, 138*, 109948. https://doi.org/10.1016/j.chaos.2020.109948
[19] Shayak, B., Sharma, M. M., Gaur, M., & Mishra, A. K. (2021). Impact of reproduction number on the multiwave spreading dynamics of COVID-19 with temporary immunity: A mathematical model. *International Journal of Infectious Diseases, 104*, 649-654.
[20] Kuddus, M. A., Mohiuddin, M., & Rahman, A. (2021). Mathematical analysis of a measles transmission dynamics model in Bangladesh with double dose vaccination. *Scientific Reports, 11*(1), 1-16.
[21] Edward, S., Raymond, K. E., Gabriel, K. T., Nestory, F., Godfrey, M. G., & Arbogast, M. P. (2015). A mathematical model for control and elimination of the transmission dynamics of measles. *Applied and Computational Mathematics, 4*(6), 396-408.
[22] Sen, M. D. L., Alonso-Quesada, S., Ibeas, A., & Nistal, R. (2021). On a discrete SEIR epidemic model with two-doses delayed feedback vaccination control on the susceptible. *Vaccines, 9*(4), 398.
[23] Gomes, M. G. M., Ferreira, M. U., Corder, R. M., King, J. G., Souto-Maior, C., Penha-Gonçalves, C., et al. (2022). Individual variation in susceptibility or exposure to SARS-CoV-2 lowers the herd immunity threshold. *Journal of Theoretical Biology, 111063*. https://doi.org/10.1016/j.jtbi.2022.111063
[24] Annas, S., Pratama, M. I., Rifandi, M., Sanusi, W., & Side, S. (2020). Stability analysis and numerical simulation of SEIR model for pandemic COVID-19 spread in Indonesia. *Chaos, Solitons & Fractals, 139*, 110072. https://doi.org/10.1016/j.chaos.2020.110072
[25] Moore, S., Hill, E. M., Tildesley, M. J., Dyson, L., & Keeling, M. J. (2021). Vaccination and non-pharmaceutical interventions for COVID-19: A mathematical modelling study. *The Lancet Infectious Diseases, 21*(6), 793-802.
[26] Yang, P., Yang, G., Qi, J., Sheng, B., Yang, Y., Zhang, S., et al. (2021). The effect of multiple interventions to balance healthcare demand for controlling COVID-19 outbreaks: A modelling study. *Scientific Reports, 11*(1). https://doi.org/10.1038/s41598-021-8217
[27] Sah, P., Vilches, T. N., Moghadas, S. M., Fitzpatrick, M. C., Singer, B. H., Hotez, P. J., et al. (2021). Accelerated vaccine rollout is imperative to mitigate highly transmissible COVID-19 variants. *EClinicalMedicine, 35*, 100865. https://doi.org/10.1016/j.eclinm.2021.100865
[28] Martínez-Rodríguez, D., Gonzalez-Parra, G., & Villanueva, R. J. (2021). Analysis of key factors of a SARS-CoV-2 vaccination program: A mathematical modeling approach. *Epidemiologia, 2*(2), 140-161.
[29] Rahman, A., & Kuddus, M. A. (2021). Modelling the transmission dynamics of COVID-19 in six high-burden countries. *Biomedical Research International, 2021*, 1-17. https://doi.org/10.1155/2021/5089184
[30] Aguilar-Canto, F. J., de Leon, U.-P., & Avila-Vales, E. (2022). Sensitivity theorems of a model of multiple imperfect vaccines for COVID-19. *Chaos, Solitons & Fractals, 156*, 111844. https://doi.org/10.1016/j.chaos.2022.111844
[31] Ramos, A. M., Vela-Pérez, M., Ferrández, M. R., Kubik, A. B., & Ivorra, B. (2021). Modeling the impact of SARS-CoV-2 variants and vaccines on the spread of COVID-19. *Communications in Nonlinear Science and Numerical Simulation, 102*, 105937. https://doi.org/10.1016/j.cnsns.2021.105937
[32] Arruda, E. F., Das, S. S., Dias, C. M., Pastore, D. H., & Khudyakov, Y. E. (2021). Modelling and optimal control of multi strain epidemics, with application to COVID-19. *PLoS ONE, 16*(9), e0257512.
[33] de Leon, U.-P., Avila-Vales, E., & Huang, K.-L. (2022). Modeling COVID-19 dynamics in Mexico with vaccination. *Chaos, Solitons & Fractals, 157*, 111927. https://doi.org/10.1016/j.chaos.2022.111927
[34] Dubey, R. K., Pandey, R., & Rajbhar, J. (2024). A mathematical model on COVID-19 studying the efficacy of testing to control the epidemics. *Obstetrics & Gynecology*.

[35] Dubey, R. K., & Pandey, R. (2024). Mathematical strategies using differential equations for controlling Nipah virus and COVID-19: A combined study. *Tuijin Jishu/Journal of Propulsion Technology, 45*(2), 250-264.